JOURNAL OF COMPUTATIONAL PHYSICS **137,** 186–211 (1997)
ARTICLE NO. CP975799

A Spectral Solver for the Navier–Stokes Equations in the Velocity–Vorticity Formulation for Flows with Two Nonperiodic Directions

H. J. H. Clercx

Department of Physics, Eindhoven University of Technology, P.O. Box 513, 5600 MB Eindhoven, The Netherlands
E-mail: clercx@tns.phys.tue.nl

Received December 19, 1996; revised July 16, 1997

A novel pseudospectral solution procedure for the Navier–Stokes equations in the velocity–vorticity formulation, suitable to simulate flows with two nonperiodic directions, is proposed. An influence matrix method, including a tau correction procedure, has been employed to elicit an algorithmic substitute for the *a priori* lacking boundary conditions for the vorticity. Following O. Daube (*J. Comput. Phys.* **103,** 402 (1992)) the influence matrix is built by enforcing either the definition of the vorticity or the continuity equation at the boundary of the domain. The influence matrix is nonsingular in both cases. The order of the influence matrix is twice larger than one would expect from analogous solution methods based on finite differences or finite elements. The spatial discretization is based on a 2D Chebyshev expansion on a *nonstaggered* grid of collocation points, and the boundary conditions are imposed via the Lanczos tau procedure. The time marching scheme is Adams–Bashforth for the advection term and Crank–Nicolson for the viscous term. The proposed scheme yields machine accurate divergence–free flow fields, and the definition of the vorticity is satisfied within machine accuracy.

Key Words: Chebyshev expansion; influence matrix; pseudospectral method; tau correction; velocity–vorticity approach.

1. INTRODUCTION

In recent years several studies appeared on the numerical solution of the (unsteady) Navier–Stokes equations in the velocity–vorticity ($\mathbf{u}$, ω) formulation [1–11].

0021-9991/97 $25.00

All these numerical solution procedures are based on finite difference or finite element techniques for the spatial discretization of the Navier–Stokes equations. It is remarkable that thus far no attempts to solve the velocity–vorticity equations with spectral or pseudospectral methods have been reported in the literature, although hybrid techniques are known where finite differences are used in two directions and Fourier modes are employed for the third direction. Spectral methods are becoming an increasingly popular tool for the investigation of fundamental processes in fluid dynamics such as the transition to turbulence in flow phenomena like boundary layers, mixing layers, and free shear layers, but also for fundamental studies of 2D and 3D homogeneous isotropic turbulence. The advantages of employing spectral methods in the investigation of these phenomena are the exponential convergence behaviour and the strongly reduced numerical damping and dispersion properties. These properties make spectral methods particularly suited for direct numerical simulations (DNS) of turbulent flows and underlines the importance of spectral methods as a complementary tool in bridging the gap between fundamental studies of turbulence and investigations of flows with engineering relevance. Finite difference and finite element methods are generally better suited for numerical simulations of flows in complex geometries, but for such problems the spectral element method has been proposed recently and applied successfully.

The aim of the present paper is to elucidate an approach to solving the Navier–Stokes equations in the ($\mathbf{u}$, ω) formulation with a pseudospectral method based on the expansion of the components of the velocity and the vorticity in a double truncated series of Chebyshev polynomials. The discretized set of equations consists of a Helmholtz equation for the vorticity and Poisson equations for the components of the velocity. The key element is the application of an influence matrix technique in order to obtain the *a priori* unknown boundary values of the vorticity and to implement a so-called tau correction to eliminate the effects of discretization errors. The tau correction appears to be essential; a naive approach without tau correction leads to catastrophical numerical instabilities. The order of the nonsingular influence matrix is twice larger than one would expect from analogous solution methods based on finite differences or finite elements, but is the same as the order for the influence matrix applied in pseudospectral methods based on the primitive variable formulation of the Navier–Stokes equations [12].

For the (numerical) investigation of vortex dominated flows it appeared that the velocity–vorticity formulation of the Navier–Stokes equations is often the most appropriate choice. An important reason is that in such flows the advection of vorticity is one of the most important processes determining the flow dynamics, and studying such flows in terms of vorticity and velocity is closer to physical reality. A few more arguments in favour of the ($\mathbf{u}$, ω) formulation can be found in the literature. For example, as already indicated by some authors [10, 11], the treatment of the boundary conditions might be easier in some specific situations. An example is that of external flows where the boundary conditions at infinity are easier to implement for the vorticity than for the pressure. Another advantage shows up when this method is applied to problems in a noninertial frame of reference. As discussed by Speziale [13], it can be shown that the noninertial effects only enter into the solution procedure of the velocity–vorticity equations via the (proper)

implementation of the initial and boundary conditions. As a consequence, the general applicability of a numerical algorithm based on the ($\mathbf{u}$, ω) formulation is enhanced compared to other formulations; it is independent of whether or not the frame of reference is inertial. Finally, the most natural relation between vortex and particle methods on the one hand and the Navier–Stokes equations on the other is the velocity–vorticity formulation of the latter. This has advantages in studying the inviscid limit of the Navier–Stokes equations (Euler equations), or it results eventually in a better understanding of vortex methods near no-slip boundaries. A disadvantage of the velocity–vorticity formulation, compared with the primitive variable formulation, is that in the most general three-dimensional case the ($\mathbf{u}$, ω) formulation requires more equations (total six) to be solved than the primitive variable formulation (total four). However, this constraint on the ($\mathbf{u}$, ω) formulation can be relaxed when the flow is periodic in at least one direction, or when particular techniques are used as described recently by Shen and Loc [14]. In their simulations of 3D flows around a cube or a sphere with a finite difference scheme, they solved, besides the vorticity transport equation for the three components of the vorticity, only two Poisson equations for the velocity. The third component was obtained by using the continuity equation. Additionally, the use of parallel processors makes the number of elliptic equations, which have to be solved in either the primitive variable or the velocity–vorticity formulation, of minor importance. Several relevant aspects concerning numerical simulations of incompressible viscous flows are discussed in Quartapelle [11], where the crucial issue of the boundary conditions is also investigated in detail.

First results of numerical simulations of the unsteady Navier–Stokes equations based on the velocity–vorticity formulation were reported by Fasel [1], who investigated the stability of boundary layers in two dimensions by a finite difference model. The approach used by Fasel consists of solving a parabolic equation for the vorticity and Poisson equations for the velocity field. Dennis, Ingham, and Cook [2] presented results of a numerical study of three-dimensional steady flows which was also based on finite difference techniques. Another approach, based on compact finite difference schemes, has been introduced by Gatski, Grosch, and Rose [3, 4]. In their study of the flow in 2D driven square and rectangular cavities the vorticity equation has been solved, together with two first-order partial differential equations, viz. the continuity equation and the definition of the vorticity. More recently several numerical recipes have been devised to solve the steady state 3D Navier–Stokes equations for flows in a cubic cavity [6, 8]. Subsonic internal flow problems have also been studied with the velocity–vorticity approach. With a finite element solution of the 3D compressible Navier–Stokes equations Guevremont *et al.* [9] have investigated the steady state flow in a cubic cavity for several Mach numbers. These 3D flow simulations have all been restricted to quite low Reynolds numbers due to fast-growing computational cost with increasing Reynolds number.

Organization of this paper is as follows: in the following section we recall the governing equations in dimensionless form, the time discretization scheme, and the spatial approximation by a Chebyshev pseudospectral method. In Section 3 the application of the influence matrix technique, based on enforcing the definition of the vorticity on the boundary, in the form proposed by Daube [10], is discussed.

The tau correction for the vorticity is then proposed in Section 4. Again along Daube's work, an alternative approach, based on enforcing the continuity equation on the boundary, is discussed in Section 5. We conclude with a brief discussion and summary of the results.

2. DISCRETIZATION OF THE GOVERNING EQUATIONS

2.1. *Formulation of the Problem*

We consider a two-dimensional square domain D with boundary ∂D. The Cartesian coordinates in a frame of reference are denoted by x and y. The equation governing the nondimensional (scalar) vorticity is obtained by taking the curl of the momentum equation and has the form

$$\frac{\partial \omega}{\partial t} + (\mathbf{u} \cdot \nabla)\omega = \frac{1}{\mathrm{Re}} \nabla^2 \omega \quad \text{in } D, \tag{1}$$

where $\mathbf{u} = (u, v)$ and $\omega = \partial v/\partial x - \partial u/\partial y$ are the dimensionless velocity vector and the vorticity, respectively. The Reynolds number is defined as $\mathrm{Re} = UL/\nu$ with U a characteristic velocity, L a characteristic length scale, and ν the kinematic viscosity. The vorticity equation (1) must be combined with the definition of the vorticity and the continuity equation, as well as the boundary conditions for the velocity,

$$\begin{aligned} \mathbf{k} \cdot \nabla \times \mathbf{u} &= \omega \quad \text{in } D, \\ \nabla \cdot \mathbf{u} &= 0 \quad \text{in } D, \\ \mathbf{u} &= \mathbf{u}_\mathrm{b} \quad \text{on } \partial D, \end{aligned} \tag{2}$$

where the unit vector $\mathbf{k}$ is normal to the flow domain. An initial condition, $\omega|_{t=0} = \mathbf{k} \cdot \nabla \times \mathbf{u}_0$, where $\mathbf{u}_0$ is the initial velocity field, is also supplemented. Furthermore, the boundary velocity $\mathbf{u}_\mathrm{b}$ has to satisfy a compatibility condition which follows from the integration of the continuity equation over the domain D, applying the divergence theorem, and using the velocity boundary condition, resulting in

$$\int_{\partial D} \mathbf{n} \cdot \mathbf{u}_\mathrm{b}\, ds = 0, \tag{3}$$

where $\mathbf{n}$ is the unit vector normal to the boundary and ds denotes the length of an infinitesimal element of the boundary ∂D.

In solving the vorticity equation (1), together with Eq. (2), the difficulty is that there is no boundary condition for the vorticity at solid walls since the no-slip condition for the velocity cannot be reformulated in equivalent conditions of boundary value type for the vorticity. Special methods have to be employed in order to determine the boundary value of the vorticity, which range from approximate techniques based on interpolation to more satisfactory methods relying upon a rigorous mathematical foundation such as the influence matrix method and the application of vorticity integral conditions [11]. An example of the latter approach

was recently reported by Nguyen, Paik, and Chung [15] who applied this method to incompressible flows with two nonperiodic directions in the stream function–vorticity formulation.

Daube [10] has shown that the formulation of the equations of motion in the form presented by Eqs. (1) and (2) is mathematically equivalent to the set consisting of the vorticity equation (1), together with the relations:

$$\begin{aligned} \mathbf{k} \cdot \nabla \times \mathbf{u} &= \omega && \text{on } \partial D, \\ \nabla^2 \mathbf{u} &= \mathbf{k} \times \nabla \omega && \text{in } D, \\ \mathbf{u} &= \mathbf{u}_b && \text{on } \partial D. \end{aligned} \tag{4}$$

For the details we refer to the paper by Daube [10]. Our approach will be based on the set of Eqs. (1) and (4).

2.2. *Time Discretization*

The time discretization of the vorticity equation considered in this work is semi-implicit and uses the explicit Adams–Bashforth scheme for the advection term and the implicit Crank–Nicolson procedure for the diffusive term—a combination generally referred to as the ABCN scheme. The time-discretized equations based on the ABCN scheme, where the superscript denotes the time-level at which the variables are considered (for example, $\omega^{n+1} = \omega((n+1)\Delta t)$) are

$$\begin{aligned} (\nabla^2 - \lambda)\,\omega^{n+1} &= S^{n,n-1} && \text{in } D, \\ \nabla^2 \mathbf{u}^{n+1} &= \mathbf{k} \times \nabla \omega^{n+1} && \text{in } D, \\ \mathbf{u}^{n+1} &= \mathbf{u}_b^{n+1} && \text{on } \partial D, \\ \mathbf{k} \cdot \nabla \times \mathbf{u}^{n+1} &= \omega^{n+1} && \text{on } \partial D, \end{aligned} \tag{5}$$

where $\lambda = 2\mathrm{Re}/\Delta t$. The quantity $S^{n,n-1}$, with $n \geq 1$, includes only terms already known,

$$S^{n,n-1} = -(\nabla^2 + \lambda)\omega^n + \mathrm{Re}[3(\mathbf{u} \cdot \nabla \omega)^n - (\mathbf{u} \cdot \nabla \omega)^{n-1}]. \tag{6}$$

An alternative time discretization must be used for the first time integration step in order to keep the overall time integration scheme second-order accurate. We can conclude that, thanks to the time discretization, the set of Eqs. (1) and (4) is reduced to a linear set and that the vorticity and velocity fields may be determined by solving elliptic equations when the boundary conditions are known.

2.3. *Spatial Approximation*

The flow domain of interest is a two-dimensional square cavity of width L—in dimensionless form the square $[-1, 1] \times [-1, 1]$. No-slip boundary conditions for the velocity are assumed which requires a high resolution near the solid boundaries of the container. This requirement is satisfied by employing a pseudospectral method

based on the expansion of the relevant flow parameters in terms of Chebyshev polynomials $T_n(x)$ which have the property that the zeros of these polynomials condense near the boundaries (the distance between adjacent zeros of $T_n(x)$ near the boundary is $O(n^{-2})$). The vorticity and both components of the velocity are expanded in a double-truncated series of Chebyshev polynomials, i.e.,

$$\omega(x, y, t) = \sum_{n=0}^{N} \sum_{m=0}^{M} \hat{\omega}_{nm}(t)\, T_n(x)\, T_m(y), \tag{7}$$

$$\mathbf{u}(x, y, t) = \sum_{n=0}^{N} \sum_{m=0}^{M} \hat{\mathbf{u}}_{nm}(t)\, T_n(x)\, T_m(y), \tag{8}$$

where the Chebyshev polynomials $T_n(x) = \cos(n\theta)$ with $\theta = \cos^{-1}(x)$. For convenience the number of Chebyshev polynomials in these expansions are always chosen such that N and M are even. By using the orthogonality relationships for Chebyshev polynomials, based on employing a collocation procedure at the Chebyshev–Gauss–Lobatto points, the expansion coefficients are obtained [16]. Transformations from physical space to the spectral space of expansion coefficients, and vice versa, can be performed efficiently by employing fast Fourier transform (FFT) methods [17]. For more details about the use of Chebyshev polynomials in spectral methods the reader can consult Canuto *et al.* [16].

All calculations, except the evaluation of the nonlinear terms, are performed in spectral space; i.e., the coefficients $\hat{\omega}_{nm}(t)$ and $\hat{\mathbf{u}}_{nm}(t)$ are marched in time. FFT methods are used to evaluate the nonlinear terms following the procedure designed by Orszag [18], where the padding technique has been used for de-aliasing (the FFT employed is based on the primes 2, 3, and 5). Both the Helmholtz and Poisson equations (see Eq. (5)) can be solved very efficiently with the Haidvogel–Zang algorithm [19]. The boundary conditions are imposed with the Lanczos tau method by dropping the last two equations corresponding to the two highest modes of the Chebyshev expansion in each direction and by evaluating the coefficients of the last two modes explicitly in terms of the boundary values (see for details Refs. [16, 19, 20]). Numerical simulations are made more efficient concerning CPU time and memory requirements by employing an even–odd decoupling of the complete algorithm (especially the elliptic solvers, the first and second derivative operators, the Chebyshev FFTs, and the influence matrix).

3. THE INFLUENCE MATRIX BY ENFORCING THE VORTICITY DEFINITION

3.1. *Introduction*

The time discretized version of the vorticity equation is a linear elliptic partial differential equation and it can be solved straightforwardly, provided that the boundary condition for the vorticity is known. However, this boundary condition is not available *a priori* and the vorticity boundary values are evaluated as a part of the solution at each time step during time integration. The approach which we have used to obtain the correct boundary values for the vorticity is the influence matrix method. This method has already been used in previous studies to resolve the lack

of boundary conditions for the pressure in simulations employing the primitive variable formulation. Examples are the numerical investigations of plane channel flow with one nonperiodic direction by Kleiser and Schumann [21], flows in cylindrical geometries such as Taylor–Couette flow by Marcus [22], natural convection in 2D cavities by Le Quéré and Alziary de Roquefort [23], non-Boussinesq convection by Le Quéré, Masson, Perrot [24], driven cavity flows by Madabhushi, Balachandar, and Vanka [12]. The study of Daube [10] is an example of the use of an influence matrix method in relation with the $(\mathbf{u}, \omega)$ formulation of the equations of motion, with the spatial discretization based on finite differences.

Influence matrix techniques, originally due to Kleiser and Schumann [21] (for a minor but important modification, see Werne [25]) are essentially based on the superposition principle for linear problems. Application of this principle offers the possibility to find solutions for elliptic problems with unknown boundary conditions by considering the solution as a superposition of simple elementary problems with known boundary conditions. The weight of each elementary solution is chosen in a self-consistent way, satisfying some auxiliary conditions for the total solution such as the definition of the vorticity and the requirement that the flow should be divergence-free. Daube has shown how to implement this method for the velocity–vorticity approach by showing that enforcement of the definition of the vorticity on the boundary of the domain is mathematically sufficient to ensure the definition of the vorticity in the domain itself. The same requirement is proved to be sufficient to ensure that the velocity field is divergence-free in the domain and on the boundary. We give a short outline of his approach in order to be self-contained.

3.2. *Enforcement of the Definition of the Vorticity*

The Poisson equations for the velocity field are derived by taking the curl of the definition of the vorticity, i.e. $\nabla \times (\nabla \times \mathbf{u}) = \nabla \times (\omega \mathbf{k})$, subsequently using the vector relation defining the Laplacian of a vector field, $\nabla^2 \mathbf{u} = \nabla(\nabla \cdot \mathbf{u}) - \nabla \times (\nabla \times \mathbf{u})$, and the assumption that the velocity field is divergence-free. The other way around, the combination of the vorticity equation and Poisson equations for the components of the velocity to obtain the flow field does not yield *a priori* equivalent solutions as the original problem formulated by Eqs. (1) and (2), due to absence of the correct vorticity boundary condition. There exists even an infinite number of solutions of the vorticity equation combined with the Poisson equations, and ω is not necessarily the vorticity of $\mathbf{u}$, i.e. $\mathbf{k} \cdot \nabla \times \mathbf{u} = \zeta$, with $\zeta \neq \omega$. In addition, the resulting velocity field is also not necessarily divergence-free. In order to obtain a divergence-free velocity field which also satisfies the vorticity definition, the following equation must be enforced:

$$\nabla^2 \mathbf{u} = \nabla(\nabla \cdot \mathbf{u}) + \mathbf{k} \times \nabla \zeta = \mathbf{k} \times \nabla \omega. \tag{9}$$

Following Daube we take the cross product of (9) with $\mathbf{k}$ and take the divergence of the resulting equation. We then arrive at

$$\nabla^2(\zeta - \omega) = 0 \quad \text{in } D. \tag{10}$$

By known properties of harmonic functions, satisfying the requirement $\zeta = \omega$ in the domain, it suffices to demand that $\zeta = \omega$ on the boundary of the domain. Daube has also proved that when $\zeta = \omega$ on the boundary of the domain, the velocity field is divergence-free.

Enforcement of the definition of the vorticity on the boundary of the domain will be performed by the influence matrix method. Suppose that the vorticity and velocity fields can be written in terms of a particular solution and a set of complementary solutions

$$\omega = \hat{\omega} + \sum_{i=1}^{P} \alpha_i \overline{\omega}_i, \quad \mathbf{u} = \hat{\mathbf{u}} + \sum_{i=1}^{P} \alpha_i \overline{\mathbf{u}}_i, \tag{11}$$

where the summation $i = 1$ to P represents all the boundary points, excluding the corner points, in some sequential manner with $P = 2N + 2M - 4$ for the total number of relevant boundary points. The corner points can be excluded because the vorticity at the corners is automatically equal to zero, due to the absence of a normal component of the flow on the boundary. It should be emphasized that this treatment of the four corner values of the vorticity is basically a pragmatic choice and is not entirely justified mathematically. The particular solutions $\hat{\omega}$ and $\hat{\mathbf{u}}$ are obtained by using an arbitrary boundary condition for the vorticity to solve Eq. (5); the most obvious two are putting $\hat{\omega} = 0$ or using the boundary values of the vorticity obtained at the preceding time step. With the calculated vorticity field the velocity can be obtained by solving the Poisson equations. As stated before, the resulting flow field is not divergence-free and $\mathbf{k} \cdot \nabla \times \mathbf{u} = \zeta \neq \omega$. The complementary solutions for the vorticity are solutions of the vorticity equation with zero source term and with zero boundary conditions, except at one of the boundary nodes where it equals one. Subsequently the Poisson equations for the corresponding velocity field are solved. Summarizing, $\overline{\omega}_i$ and $\overline{\mathbf{u}}_i$ are solutions of the set of equations,

$$\begin{aligned} (\nabla^2 - \lambda)\overline{\omega}_i &= 0 && \text{in } D \text{ with } \overline{\omega}_i(\gamma_j) = \delta_{ij} \text{ on } \partial D, \\ \nabla^2 \overline{\mathbf{u}}_i &= \mathbf{k} \times \nabla \overline{\omega}_i && \text{in } D, \\ \overline{\mathbf{u}}_i &= 0 && \text{on } \partial D, \end{aligned} \tag{12}$$

where i is running from 1 to P, γ_j are the respective boundary nodes excluding the corners, and δ_{ij} is the Kronecker symbol. All coefficients α_i are obtained by demanding $\mathbf{k} \cdot \nabla \times \mathbf{u} = \omega$ on the boundary. Using Eq. (11) this yields

$$(\hat{\zeta} - \hat{\omega})_j + \sum_{i=1}^{P} \alpha_i (\overline{\zeta}_i - \overline{\omega}_i)_j = 0 \quad \forall j \in \{1, ..., P\}, \tag{13}$$

where $(\overline{\zeta}_i - \overline{\omega}_i)_j \equiv M_{ji}$ are the elements of the influence matrix $\mathbf{M}$. The coefficients α_i, which are the unknown values of the vorticity on the boundary nodes, are determined via

$$\alpha_i = -\sum_{j=1}^{P} (\mathbf{M}^{-1})_{ij} (\hat{\zeta} - \hat{\omega})_j. \tag{14}$$

At this stage the correct boundary values for the vorticity are known and the set of Eqs. (5) can be solved, again, now using the new vorticity distribution on the boundary.

This approach, without application of a tau correction to remove discretization errors, appears to be numerically unstable. It is noteworthy that an analogous approach applied to the Navier–Stokes equations in primitive variables does not lead to numerical instabilities, although the velocity field is not divergence-free.

4. TAU CORRECTION FOR THE VORTICITY

The reason for the numerical instabilities appears to be that, despite the fact that the definition of the vorticity is satisfied within machine accuracy on the boundary of the domain, it is not in the interior. This observation leads also to the conclusion that the flow cannot be divergence-free. Both observations seem to contradict the theoretical analysis presented by Daube, which can be explained in the following way: the solution procedure for Poisson or Helmholtz equations in spectral space does not make use of the highest frequency modes of the spectral representation of the source term. This is due to imposing the boundary conditions via the (Lanczos) spectral tau method. For details of the implementation of the spectral tau method, particularly the treatment of the high frequency modes, the reader is referred to, e.g., Canuto *et al.* [16], Haidvogel and Zang [19], and Tuckerman [20]. As a consequence of applying the tau method the elliptic partial differential equations (for example, those presented in Eq. (5)) are not satisfied numerically for the highest frequency modes, or, conversely, substituting the solution in the original differential equation does not yield high frequency modes which agree with those of the corresponding source term. Let us illustrate the problem with the Poisson equations for the velocity field. The numerical equivalent of Eq. (9) can be formulated as $\nabla^2\mathbf{u} = \mathbf{k} \times \nabla\omega + \boldsymbol{B}$, with $\boldsymbol{B}$ the representation in physical space of the highest frequency modes. The Chebyshev expansion coefficients $\hat{\boldsymbol{B}}_{nm}$ are zero for $n \leq N - 2$ and $m \leq M - 2$. The nonzero modes of $\hat{\boldsymbol{B}}_{nm}$ are usually referred to as high frequency residuals, and the solution of the Poisson equations is independent of the particular values of the high frequency residuals. As a consequence the velocity field is independent of $\boldsymbol{B}$. However, the appearance of high frequency residuals when applying spectral tau methods make straightforward employment of the theoretical analysis presented by Daube impossible; a modification is necessary. The same difficulties arise for collocation methods (see, e.g., Refs. [20, 12]) and also when the primitive variable formulation $(\mathbf{u}, p)$ is employed (high frequency residuals in the momentum equations contaminate the Poisson equation for the pressure). The approach to solving this kind of numerical problems is to impose a so-called tau correction in order to adjust these discretization errors.

Consider the Poisson equations for the velocity field, Eq. (9). Anticipating imposing a tau correction, this equation should be rewritten in the form

$$\nabla^2\mathbf{u} = \nabla(\nabla \cdot \mathbf{u}) + \mathbf{k} \times \nabla\zeta = \mathbf{k} \times \nabla\omega + \boldsymbol{B}, \tag{15}$$

where $\boldsymbol{B}$ is *a priori* unequal to zero. These modes do not affect the velocity field $\mathbf{u}$ itself. Following the procedure suggested by Daube we obtain

$$\nabla^2(\zeta - \omega) = -\nabla \cdot (\mathbf{k} \times \boldsymbol{B}), \tag{16}$$

which is evidently not a Laplace equation but a Poisson equation. Although the high frequency modes do not affect the velocity field they do affect the difference between ζ and ω, because of the appearance of low frequency modes due to differentiation of $\boldsymbol{B}$ in Eq. (16) (differentiation of a Chebyshev polynomial of degree n results in the appearance of Chebyshev polynomials of lower degree). Consequently, the term $-\nabla \cdot (\mathbf{k} \times \boldsymbol{B}) = \mathbf{k} \cdot \nabla \times \boldsymbol{B}$ acts as a source term, and Daube's procedure, based on using the maximum principle for Laplace equations, is no longer effective. This difficulty can be resolved by demanding that the high frequency modes which give low frequency contributions to the RHS of Eq. (16) should be zero. The solution ($\mathbf{u}$, ω) should satisfy this demand self-consistently (see Eq. (15)). The relevant modes with low frequency contributions in the source term of Eq. (16) are: $B_x = T_n(x)T_m(y)$, with $0 \le n \le N - 2$ and m equal to $M - 1$ or M, and $B_y = T_n(x)T_m(y)$, with n equal to $N - 1$ or N and $0 \le m \le M - 2$.

The following procedure has been devised to eliminate these particular high frequency residuals of $\boldsymbol{B}$. As a first step the vorticity equation is modified by including an additional source term, $\mathbf{k} \cdot \nabla \times \mathbf{B}$, with $\mathbf{B}$ *a priori* unknown high frequency modes,

$$(\nabla^2 - \lambda)\omega = S + \mathbf{k} \cdot \nabla \times \mathbf{B}, \tag{17}$$

i.e. an adapted version of Eq. (5) [26]. Together with the unknown boundary conditions for the vorticity, the high frequency modes $\mathbf{B}$ have to be determined. This should be done in such way that the relevant high frequency modes $\boldsymbol{B}$ in the Poisson equations for the velocity field are equal to zero self-consistently; i.e., the solution $\mathbf{u}$ must satisfy: $\nabla^2\mathbf{u} - \mathbf{k} \times \nabla\omega \equiv \mathbf{0}$. Actually, an analogous procedure to adjust for discretization errors when solving the Navier–Stokes equations in the ($\mathbf{u}$, p) formulation with a collocation method has been proposed recently by Madabhushi, Balachandar, and Vanka [12]. The discretization errors appearing in their approach are due to the fact that the differential equations are not satisfied on the boundary of the domain. A thorough mathematical analysis of the application of tau and collocation corrections has been presented by Tuckerman [20].

Elimination of $\boldsymbol{B}$ can be achieved by writing the vorticity and velocity fields in terms of a particular solution and two sets of complementary solutions,

$$\omega = \hat{\omega} + \sum_{i=1}^{P} \alpha_i \overline{\omega}_i + \sum_{i=1}^{Q} \beta_i \overline{\overline{\omega}}_i \tag{18}$$

and

$$\mathbf{u} = \hat{\mathbf{u}} + \sum_{i=1}^{P} \alpha_i \overline{\mathbf{u}}_i + \sum_{i=1}^{Q} \beta_i \overline{\overline{\mathbf{u}}}_i, \tag{19}$$

with $P = 2N + 2M - 4$ for the total number of boundary points excluding the corner points, where $\omega \equiv 0$, and Q for the total number of relevant high frequency modes. The particular solutions and the first set of complementary solutions are obtained as explained in Section 3. The second set of complementary functions for the vorticity are solutions of the vorticity equation with zero source term S and with zero boundary conditions. Furthermore, all high-frequency modes are set equal to zero, except specific combinations (the specific choice will be discussed below). Subsequently, the Poisson equations for the corresponding velocity field can be solved. As might be expected, the curl of the velocity field is not equal to the vorticity $\overline{\overline{\omega}}_i$. Summarizing, $\overline{\overline{\omega}}_i$ and $\overline{\overline{\mathbf{u}}}_i$ are solutions of the set of equations,

$$\begin{aligned} (\nabla^2 - \lambda)\overline{\overline{\omega}}_i &= \mathbf{k} \cdot (\nabla \times \mathbf{b}_i) \quad \text{in } D, \text{ with } \overline{\overline{\omega}}_i = 0 \text{ and } \partial D, \\ \nabla^2 \overline{\overline{\mathbf{u}}}_i &= \mathbf{k} \times \nabla \overline{\overline{\omega}}_i \quad \text{in } D, \\ \overline{\overline{\mathbf{u}}}_i &= 0 \quad \text{on } \partial D, \end{aligned} \tag{20}$$

where the yet unspecified $\mathbf{b}_i$, with $i = 1, ..., Q$, are the high frequency modes which are subsequently excited. It is not difficult to see that not all high frequency modes $\mathbf{b} = (b_x, b_y)$ are important. Modes of b_x containing products of $T_m(y)$ with $T_{N-1}(x)$ or $T_N(x)$ remain, after differentiation with respect to y, high frequency modes and do not affect the solution of the vorticity. The other modes, containing products of $T_n(x)$ with $T_{M-1}(y)$ or $T_M(y)$, yield, after differentiation with respect to y, low frequency modes. The numerically relevant high frequency modes are $b_x = T_n(x)T_m(y)$ with $0 \le n \le N - 2$ and m equal to $M - 1$ or M. Using analogous reasoning one can show that the relevant high frequency modes b_y are represented by $b_y = T_n(x)T_m(y)$, with n equal to $N - 1$ or N and $0 \le m \le M - 2$. The total number of relevant high frequency modes is thus $2N + 2M - 4$. However, four special linear combinations of high frequency modes exist which can be identified as an irrotational part of $\mathbf{B}$. These linear combinations will not affect the vorticity field via Eq. (17) and are thus useless for the adjustment procedure of $\boldsymbol{B}$. Without filtering these modes the resulting influence matrix is singular; it has four zero eigenvalues. Special procedures exist to circumvent these difficulties [20]. However, when we reduce the number of excited high-frequency modes by four in such way that none of the linear combinations of the remaining modes is irrotational ($\nabla \times \mathbf{B} \neq \mathbf{0}$), the influence matrix is invertible. The total number of relevant high frequency modes reduces to $Q = 2N + 2M - 8$. The specific implementation for adjusting the influence matrix in order to avoid irrotational modes of $\mathbf{B}$ is rather arbitrary; in the present case the high frequency modes $T_s(x)T_{M-1}(y)$ and $T_s(x)T_M(y)$, with $s = 0$ or 1, are replaced by the modes $[T_s(x) - T_{N-2-s}(x)]T_{M-1}(y)$ and $[T_s(x) - T_{N-2-s}(x)]T_M(y)$, respectively. Furthermore, the modes $T_{N-2-s}(x)$ $T_{M-1}(y)$ and $T_{N-2-s}(x)T_M(y)$ are not excited when building the influence matrix.

Coefficients α_i and β_i are obtained by simultaneously putting $\mathbf{k} \cdot \nabla \times \mathbf{u} = \omega$ at all boundary nodes and requiring that all (relevant) high frequency modes in the Poisson equations for the velocity field are self-consistently equal to zero. The following set of equations (with j running over the appropriate values) for the coefficients α_i and β_i should then be solved to satisfy these requirements,

$$(\hat{\zeta} - \hat{\omega})_j + \sum_{i=1}^{P} \alpha_i (\bar{\zeta}_i - \overline{\omega}_i)_j + \sum_{i=1}^{Q} \beta_i (\bar{\bar{\zeta}}_i - \overline{\overline{\omega}}_i)_j = 0, \tag{21}$$

$$\hat{\boldsymbol{B}}_j + \left(\sum_{i=1}^{P} \alpha_i \overline{\boldsymbol{B}}_i \right)_j + \left(\sum_{i=1}^{Q} \beta_i \overline{\overline{\boldsymbol{B}}}_i \right)_j = \mathbf{0}, \tag{22}$$

where $\hat{\boldsymbol{B}} = \nabla^2 \hat{\mathbf{u}} - \mathbf{k} \times \nabla \hat{\omega}$, $\overline{\boldsymbol{B}}_i = \nabla^2 \overline{\mathbf{u}}_i - \mathbf{k} \times \nabla \overline{\omega}_i$ (with $i = 1, ..., P$) and $\overline{\overline{\boldsymbol{B}}}_i = \nabla^2 \overline{\overline{\mathbf{u}}}_i - \mathbf{k} \times \nabla \overline{\overline{\omega}}_i$ (with $i = 1, ..., Q$) are the high frequency residuals of the Poisson equations for the components of the velocity of the particular solution and the two sets of complementary solutions, respectively. The influence matrix $\mathbf{M}$ has now the form

$$\mathbf{M} = \begin{bmatrix} M_{ji}^{11} & M_{ji}^{12} \\ M_{ji}^{21} & M_{ji}^{22} \end{bmatrix} = \begin{bmatrix} (\bar{\zeta}_i - \overline{\omega}_i)_j & (\bar{\bar{\zeta}}_i - \overline{\overline{\omega}}_i)_j \\ (\overline{\boldsymbol{B}}_i)_j & (\overline{\overline{\boldsymbol{B}}}_i)_j \end{bmatrix}, \tag{23}$$

and is a $(4N + 4M - 12) \times (4N + 4M - 12)$ matrix. The coefficients α_i, representing the boundary values of the vorticity, and β_i, the weights of the additional source terms $\mathbf{k} \cdot \nabla \times \mathbf{b}_i$ in the vorticity equation, are determined by inversion of the influence matrix,

$$\alpha_i = -\sum_{j=1}^{P} (\mathbf{M}^{-1})_{ij}^{11} (\hat{\zeta} - \hat{\omega})_j - \sum_{j=1}^{Q} (\mathbf{M}^{-1})_{ij}^{12} \hat{\boldsymbol{B}}_j, \tag{24}$$

$$\beta_i = -\sum_{j=1}^{P} (\mathbf{M}^{-1})_{ij}^{21} (\hat{\zeta} - \hat{\omega})_j - \sum_{j=1}^{Q} (\mathbf{M}^{-1})_{ij}^{22} \hat{\boldsymbol{B}}_j. \tag{25}$$

As explained in Section 3 we proceed now by determining the vorticity and velocity field by solving Eq. (5) with the correct boundary values for the vorticity and the adjusted high frequency modes.

The influence matrix is calculated in a preprocessing stage and its inverse is stored before the actual time integration procedure is started. The influence matrix can become very large when the number of modes increases. However, an even–odd decoupling of the algorithm results in four smaller influence matrices which are related with even–even, even–odd, odd–even, and odd–odd modes in the x and y directions, respectively. The size of these matrices is of the order $(N + M) \times (N + M)$, which reduces the storage requirements of the influence matrix by roughly by a factor of four.

The solution cycle during time integration can be summarized as follows:

(i) Solve for the particular solution of the vorticity, $(\nabla^2 - \lambda)\hat{\omega} = S$, with $\hat{\omega} = 0$ on ∂D;

(ii) Solve the Poisson equations to obtain the particular solution of the velocity field, $\nabla^2 \hat{\mathbf{u}} = \mathbf{k} \times \nabla \hat{\omega}$;

(iii) Compute $\hat{\zeta} = \mathbf{k} \cdot \nabla \times \hat{\mathbf{u}}$ on the boundary of the domain and the high frequency residual of the Poisson equations corresponding to the particular solution, $\hat{\boldsymbol{B}} = \nabla^2 \hat{\mathbf{u}} - \mathbf{k} \times \nabla \hat{\omega}$;

(iv) Determine the boundary values of the vorticity (α_i) and the additional source term of the vorticity equation, $\mathbf{k} \cdot \nabla \times \mathbf{B} \equiv \sum_{i=1}^{Q} \beta_i \mathbf{k} \cdot (\nabla \times \mathbf{b}_i)$;

(v) Recompute the vorticity field with the new boundary values of the vorticity and the additional source term, $(\nabla^2 - \lambda)\omega = S + \mathbf{k} \cdot \nabla \times \mathbf{B}$;

(vi) Recompute the source term of the Poisson equations, $\mathbf{k} \times \nabla\omega$, and solve for the new velocity field.

In Sections 3 and 4 an influence matrix technique has been introduced for a spectral tau approach. A naturally occurring question concerning the numerical instabilities is then: Might numerical instabilities be avoided by performing the calculations in physical space (via a Chebyshev collocation procedure) instead of spectral space? The absence of high frequency residuals when the calculations are carried out in physical space seems to support the idea that enforcing the definition of the vorticity on the boundary is a sufficient condition to obtain divergence-free flow fields without the presence of numerical instabilities. Unfortunately, the discrete spatial representation of the Poisson equations for the velocity field is not satisfied on the boundaries of the domain, i.e. $\nabla^2\mathbf{u} = \mathbf{k} \times \nabla\omega + \boldsymbol{B}$, with $\boldsymbol{B}$ in this case the so-called boundary residual (cf. Ref. [12] for a collocation correction in a Chebyshev collocation procedure for the simulation of the Navier–Stokes equations in primitive variables). Again, Daube's procedure cannot be applied in its original form, and it might be expected that the implementation of an influence matrix technique, without taking into account a correction for boundary residuals, leads to numerical instabilities.

5. THE INFLUENCE MATRIX BY ENFORCING THE CONTINUITY EQUATION

An alternative set of equations can be formulated which gives formally equivalent results as Eq. (5) [10]. This equivalent set (time discretized version) has the form

$$\begin{aligned} (\nabla^2 - \lambda)\omega &= S && \text{in } D, \\ \nabla^2\mathbf{u} &= \mathbf{k} \times \nabla\omega && \text{in } D, \\ \mathbf{u} &= \mathbf{u}_\mathrm{b} && \text{on } \partial D, \\ \nabla \cdot \mathbf{u} &= 0 && \text{on } \partial D, \\ \omega|_{t=0} &= \mathbf{k} \cdot \nabla \times \mathbf{u}_0 && \text{in } D. \end{aligned} \tag{26}$$

The vorticity field in the computational domain D should also satisfy the integral condition expressing that the vorticity integrated over the domain D is equal to the contour integral of the tangential component of the velocity along the boundary of the domain D (application of Stokes theorem),

$$\int_D \omega(x, y)\, dx\, dy = \int_{\partial D} \tau \cdot \mathbf{u}_\mathrm{b}\, ds, \tag{27}$$

where τ denotes the unit vector tangential to the boundary and ds denotes the length of an infinitesimal element of the boundary ∂D. The mathematical foundation of the present set of equations is, again, based on the enforcement of

$$\nabla^2\mathbf{u} = \nabla(\nabla \cdot \mathbf{u}) + \mathbf{k} \times \nabla\zeta = \mathbf{k} \times \nabla\omega. \tag{28}$$

After taking the divergence of (28) we arrive at

$$\nabla^2(\nabla \cdot \mathbf{u}) = 0 \quad \text{in } D, \tag{29}$$

and using the maximum-principle for Laplace equations it can be shown that it is sufficient to enforce $\nabla \cdot \mathbf{u} = 0$ on the boundary of the domain in order to enforce the continuity equation everywhere in D. When this condition is satisfied it can be shown that $\nabla(\zeta - \omega) = 0$, or equivalently, $\mathbf{k} \cdot \nabla \times \mathbf{u} - \omega$ is constant in D. But, by the integral condition (27), the constant can be shown to be zero.

Without tau correction, the approach based on enforcing the continuity equation at the boundaries is numerically unstable. Thus, as is the case when enforcing the definition of the vorticity, we have to correct for discretization errors due to the application of Lanczos tau procedure to impose the boundary conditions. The numerical equivalent of Eq. (28) is $\nabla^2\mathbf{u} = \mathbf{k} \times \nabla\omega + \boldsymbol{B}$, where $\boldsymbol{B}$ is *a priori* unequal to zero. Following the procedure suggested by Daube we obtain for the numerical equivalent of Eq. (29)

$$\nabla^2(\nabla \cdot \mathbf{u}) = \nabla \cdot \boldsymbol{B}. \tag{30}$$

The maximum principle for Laplace equations is no longer effective, and an analogous procedure as in Section 4 can be devised to circumvent these difficulties. Consider Eq. (17), $(\nabla^2 - \lambda)\omega = S + \mathbf{k} \cdot \nabla \times \mathbf{B}$. We have to find a specific $\mathbf{B}$ such that the relevant high frequency modes $\boldsymbol{B}$ are equal to zero. These modes are for this particular case: $B_x = T_n(x)T_m(y)$, with n equal to $N - 1$ or N and $0 \le m \le M - 2$, and $B_y = T_n(x)T_m(y)$, with $0 \le n \le N - 2$ and m equal to $M - 1$ or M. Note that these modes are not the same as those in Section 4. The so-called irrotational part of $\mathbf{B}$ is singled out with an analogous filtering procedure as described in Section 4, resulting in an invertible influence matrix. Introducing a particular solution and two complementary solutions of $\mathbf{u}$ and ω (Eqs. (18) and (19)) we can proceed as in Section 4. Coefficients α_i and β_i are obtained by simultaneously putting $\nabla \cdot \mathbf{u} = 0$ at all boundary nodes and requiring that all relevant high frequency modes in the Poisson equations for the velocity field are self-consistently equal to zero. The following set of equations (with j running over the appropriate values) for the coefficients α_i and β_i should then be solved to satisfy these requirements

$$(\nabla \cdot \hat{\mathbf{u}})_j + \sum_{i=1}^{P} \alpha_i (\nabla \cdot \overline{\mathbf{u}}_i)_j + \sum_{i=1}^{Q} \beta_i (\nabla \cdot \overline{\overline{\mathbf{u}}}_i)_j = 0, \tag{31}$$

$$\hat{\boldsymbol{B}}_j + \left(\sum_{i=1}^{P} \alpha_i \overline{\mathbf{B}}_i \right)_j + \left(\sum_{i=1}^{Q} \beta_i \overline{\overline{\boldsymbol{B}}}_i \right)_j = \mathbf{0}, \tag{32}$$

with $\hat{\boldsymbol{B}}$ etc. defined as below Eq. (22), $P = 2N + 2M - 4$ ($\nabla \cdot \mathbf{u} \equiv 0$ at the corners of the domain), and $Q = 2N + 2M - 8$. It is obvious that we take into account those modes which contaminate the RHS of Eq. (30) with low frequency modes. In order to satisfy the condition $\zeta = \omega$ in D, four equations of Eq. (31) have to be sacrificed (instead of one as in Daube's case) and replaced by the following conditions: $\zeta - \omega = 0$ for the Chebyshev modes (n, m) equal to (0, 0), (0, M), (N, 0), and (N, M). Enforcement of the constant mode is trivial. The need to enforce $\zeta - \omega$ for these three particular high frequency modes is due to the fact that, when applying a tau method, we effectively have to ensure that $\nabla(\zeta - \omega) = 0$ for the low frequency modes. Thus there exists still some degree of freedom for $\zeta - \omega$ which has to be enforced. Only three modes of $\zeta - \omega$ exist of which the gradients are outside the low frequency range. For simplicity, let us consider only the following combination of Chebyshev modes (related with mode (N, 0)),

$$\zeta - \omega = A\left[\frac{1}{N}T_N(x) - \frac{1}{N-2}T_{N-2}(x)\right], \tag{33}$$

where A is some arbitrary constant. It is not difficult to see that $\partial(\zeta - \omega)/\partial y = 0$ and $\partial(\zeta - \omega)/\partial x = 2AT_{N-1}(x)$; thus $\nabla(\zeta - \omega)$ has only a contribution in the high frequency range. To ensure that nevertheless $\zeta = \omega$ it has to be assured that the mode represented by Eq. (33) disappears. In the same way the other two modes of $\zeta - \omega$ are enforced. The resulting influence matrix has the desired properties in order to enforce the continuity equation and the definition of the vorticity in the domain D.

6. DISCUSSION AND CONCLUSION

All results presented in this section are based on enforcing the vorticity definition on the boundary of the computational domain. Results based on enforcing the continuity equation in the way suggested in Section 5 agree within machine accuracy with those based on enforcing the definition of the vorticity.

Before presenting some results of simulations of the 2D driven cavity and spin-up flows, we start with a summary of a more detailed assessment of the implementation of the tau correction in the algorithm which can be achieved by studying the behaviour of the divergence of the velocity field during time marching and by checking the deviation of the vorticity definition. The latter is denoted by $\delta\omega = \omega - \mathbf{k} \cdot (\nabla \times \mathbf{u})$. The divergence and $\delta\omega$ has been measured by means of an L_2-norm. The dimensionless divergence of the velocity field obtained for 2D driven cavity and spin-up flows for Re = 1000 are plotted Figs. 1a and 1b, respectively. These numerical experiments were performed with 25×25 and 33×33 Chebyshev modes. The mean dimensionless velocities for the driven cavity flow are $O(1)$, and it can therefore be concluded that the divergence of the velocity field in that example is machine accurate zero. For spin-up, the L_2-norm of the divergence is normalized by the root mean square velocity (the kinetic energy of spin-up flows always decreases in the course of time due to damping). Figures 2a and 2b provide plots of the L_2-norm of $\delta\omega$ for the same set of simulations (for spin-up, $\delta\omega$ is normalized

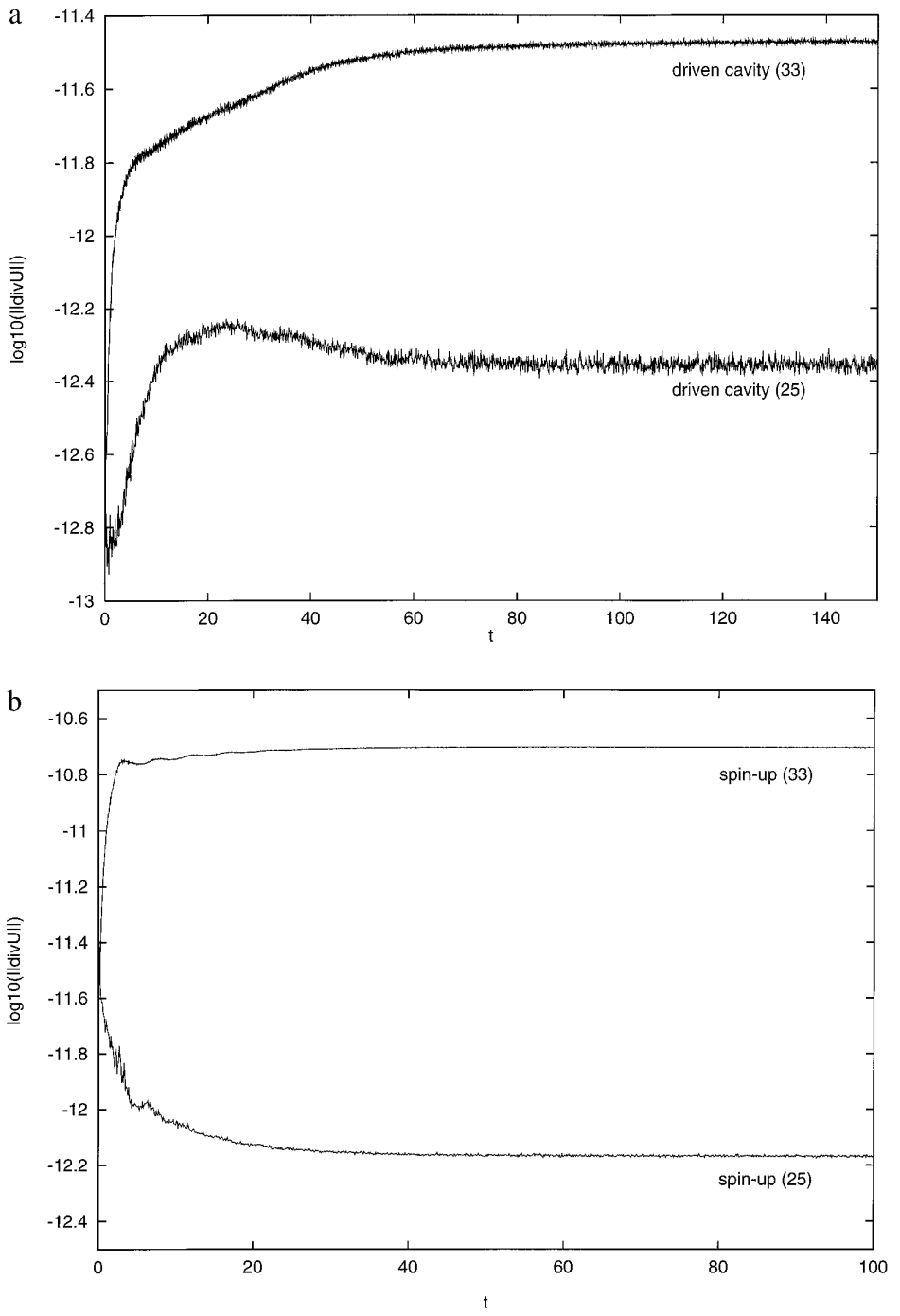

FIG. 1. The L_2-norm of the dimensionless divergence as function of dimensionless time for (a) driven cavity and (b) spin-up flows. The results for spin-up are normalized by the RMS velocity of the flow.

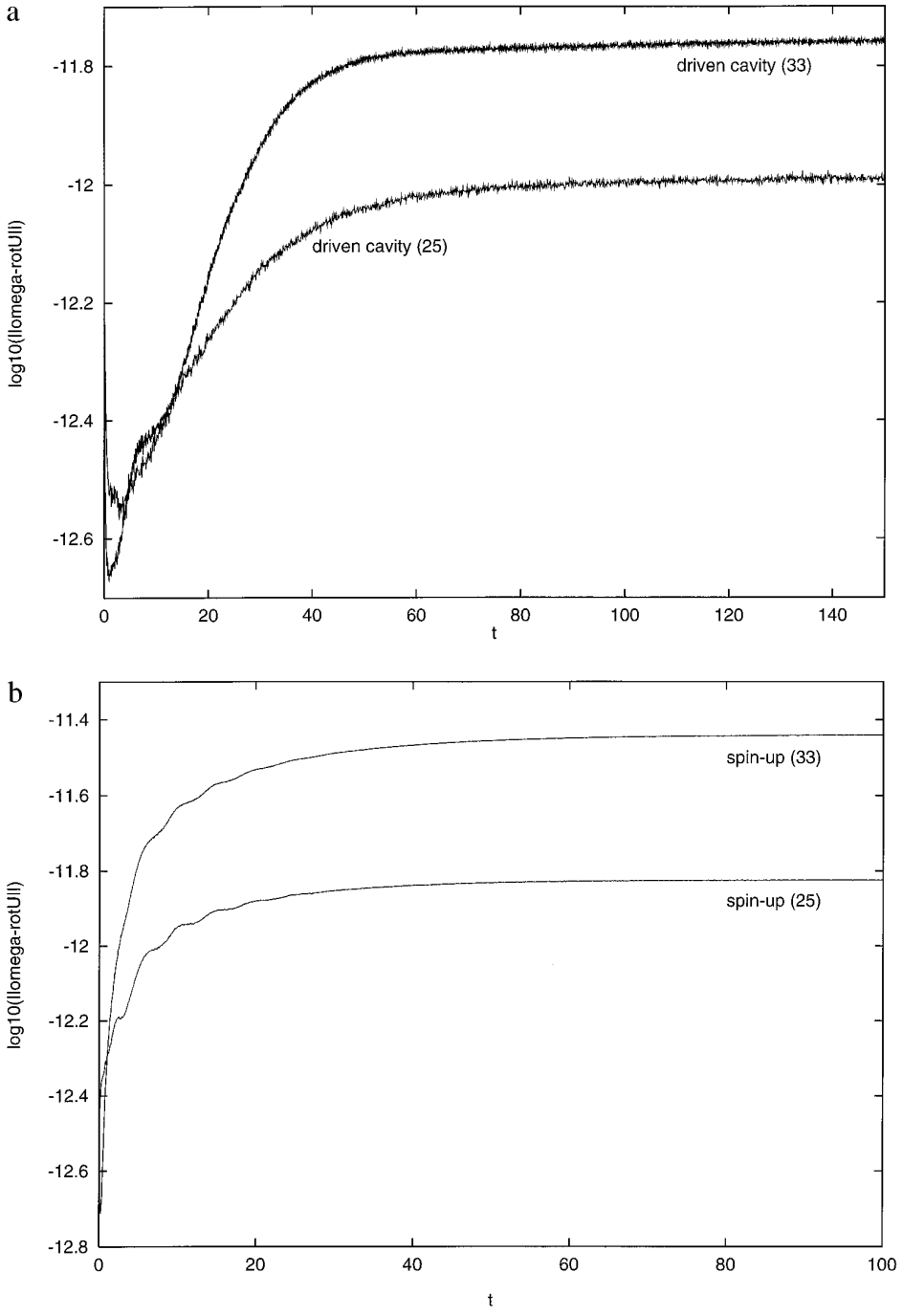

FIG. 2. The L_2-norm of the deviation of the vorticity definition $\delta\omega$ (dimensionless) as function of dimensionless time for (a) driven cavity and (b) spin-up flows. The results for spin-up are normalized by the RMS vorticity of the flow.

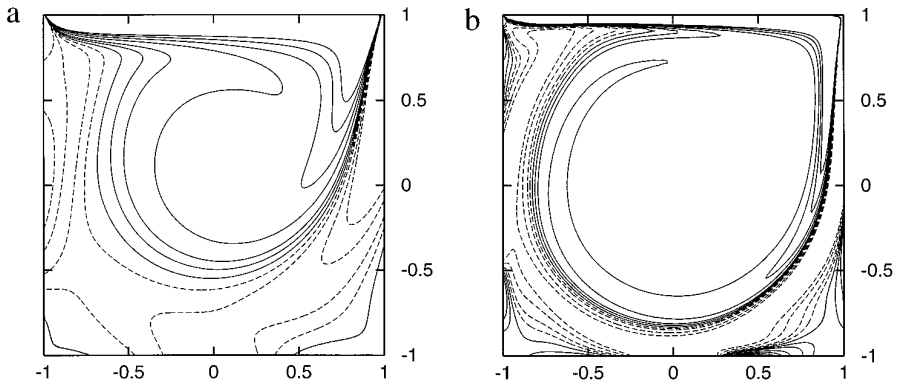

FIG. 3. The final steady state of the vorticity in the 2D driven cavity for Re = 400 (a) and Re = 3200 (b). The contour levels are chosen as in the benchmark results of Ghia *et al.* [27].

by the root mean square vorticity) and it can be concluded that also the vorticity definition is satisfied within machine accuracy. The vorticity field in the computational domain D also satisfies the integral condition expressing that the total circulation is equal, within machine accuracy, to the contour integral of the tangential component of the velocity along the boundary of the domain D.

6.1. *Flow in a Driven Cavity*

Two-dimensional flows in a square cavity with a moving (upper) lid have often been used to test numerical schemes. The main source of benchmark data is the paper by Ghia, Ghia, and Shin [27], who studied driven cavity flows for Reynolds numbers ranging from 100 to 10000 (where the Reynolds number is based on the velocity U of the moving lid and the size L of the cavity, $\mathrm{Re} = UL/\nu$). Their numerical procedure was based on the solution of the incompressible Navier–Stokes equations with a multigrid method using stream function and vorticity as dynamical variables.

We have calculated the final steady state of the flow in the 2D driven cavity for Re = 400 and Re = 3200, where a desingularization of the motion of the lid near the top corners, as proposed by Madabhushi *et al.* [12], is used. The results, which are shown in Figs. 3a–b (vorticity) and Figs. 4a–b (stream function), are in good agreement with those reported in the literature [15, 27]. The vorticity and stream function plots are based on simulations with 41 Chebyshev modes in each direction for Re = 400 and 65 Chebyshev modes in both directions for Re = 3200.

We have also compared our results with data obtained for the so-called regularized driven cavity. The horizontal speed of the upper lid of the cavity is now $u_{\mathrm{top}} = (x^2 - 1)^2$ as used by Demaret and Deville [28], Shen [29], and Phillips and Roberts [30] in previous studies. We see that $u_{\mathrm{top}} \geq 0.99$ for $|x| \leq 0.07$, thus the forcing is much weaker than in the case of the nonregularized driven cavity. This is also reflected in the total energy calculated for the final steady state; the total energy for the regularized driven cavity is roughly only half of that for the nonregularized driven cavity. The stream function and vorticity in the cavity after the steady state

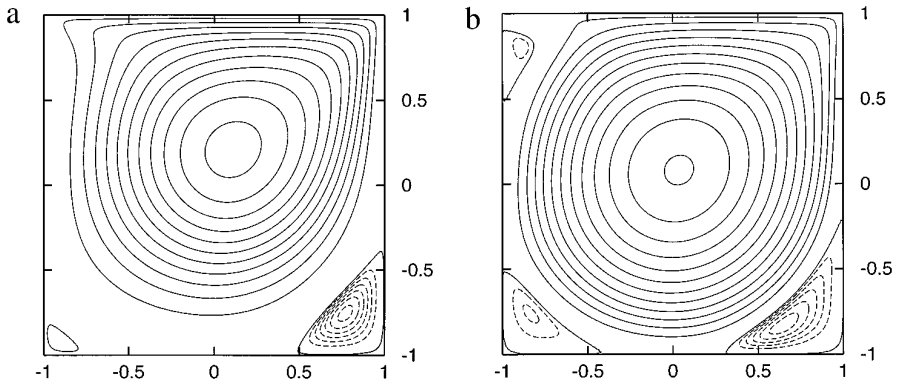

FIG. 4. The final steady state of the stream function in the 2D driven cavity for Re = 400 (a) and Re = 3200 (b). The contour levels of the stream function are plotted from $\psi = 0$ to $\psi = -0.11$ (Re = 400) or $\psi = -0.12$ (Re = 3200) with steps of 0.01 (drawn lines). The contour levels in the corner vortices (dashed lines) are from 10^{-4} to 6×10^{-4} with steps of 10^{-4} (Re = 400) and from 5×10^{-4} to 2.5×10^{-3} with steps of 5×10^{-4} (Re = 3200).

has been reached agree with the results reported in previous studies. In Table I some of our data and those from the literature concerning the position of the primary vortex, and the value of the stream function in the centre of this vortex, are summarized. Our data in Table I are converged and the number of Chebyshev modes necessary to achieve four-digit convergence are presented in the second column. For Re $\geq$ 2000 it appeared that the use of fewer Chebyshev modes than listed in Table I give still quite accurate results. For example, the position of the centre of the primary vortex and the corresponding value of the stream function in the case Re = 5000 obtained with a simulation with 37×37, instead of 65×65, Chebyshev modes are also (0.038, 0.077) and -8.81×10^{-2}, respectively. A differ-

TABLE I
Properties of the Primary Vortex of the Regularized Driven Cavity

Re	Grid	Position (x, y)	$\psi_{\max}$	Refs.
400	25×25	(0.155, 0.232)	-8.59×10^{-2}	
	17×17	(0.156, 0.250)	-8.58×10^{-2}	[29]
	24×24	(0.146, 0.242)	-8.59×10^{-2}	[30]
1000	33×33	(0.085, 0.146)	-8.72×10^{-2}	
	25×25	(0.094, 0.156)	-8.72×10^{-2}	[29]
	24×24	(0.098, 0.146)	-8.71×10^{-2}	[30]
2000	33×33	(0.059, 0.106)	-8.78×10^{-2}	
	33×33	(0.062, 0.094)	-8.78×10^{-2}	[29]
	25×25	(0.059, 0.105)	-8.78×10^{-2}	[28]
5000	65×65	(0.038, 0.077)	-8.81×10^{-2}	
	33×33	(0.032, 0.062)	-8.80×10^{-2}	[29]
	32×32	(0.050, 0.074)	-8.80×10^{-2}	[30]

Note. Compared with results from Demaret and Deville [28], Shen [29], and Phillips and Roberts [30].

ence was found in the fourth digit only. The characteristics of the secondary vortices, in the corners of the cavity, are also in good agreement with those reported in the literature.

6.2. *Two-Dimensional Spin-Up in a Square Container*

Spin-up is the adjustment process of fluid in a container, initially rotating with an angular velocity Ω, after a sudden change of the rotational velocity of the container from Ω to $\Omega + \Delta\Omega$ at $t = 0$. In a coordinate system corotating with the container one observes a large anticyclonic cell that fills the domain entirely; this motion arises because of the inability of the fluid to follow the change in rotation of the boundaries. At $t = 0^+$ boundary layers are set up and cyclonic vorticity, generated in the boundary layers, will be advected by the primary anticyclonic flow along the sides of the container. In the subsequent stage it is observed that, when the Reynolds number is large enough, boundary layer separation takes place and the advected cyclonic vorticity accumulates in small cyclonic cells in the corners of the container.

In numerical studies it appeared that spin-up simulations for intermediate and higher Reynolds numbers are quite difficult to perform. This is mainly due to the appearance of very thin boundary layers at $t = 0^+$, in which the vorticity can have large values. In order to obtain a sufficient boundary layer resolution, a quite large number of Chebyshev modes is required. The initial (dimensionless) energy of the flow is also one order of magnitude larger than in steady-state driven cavity flows; thus more interesting flow features might be expected for spin-up flows than for driven cavity flows for comparable Reynolds number. These observations led to the conclusion that simulation of spin-up flows could serve as a more critical test for pseudospectral algorithms than 2D driven cavity flows. However, no benchmark data for spin-up in square containers exist to compare our results with for this particular test.

The starting flow for 2D spin-up in a square container, with sidewalls of length L, is found by simply assuming solid-body rotation of the fluid with respect to the corotating coordinate system. The initial flow field then has the form: $\mathbf{u} = \mathbf{r} \times \Delta\boldsymbol{\Omega}$. As a result, the dimensionless vorticity in the interior at $t = 0$ is $\omega = -2$. In Figs. 5 and 6 we show two typical stages of the spin-up process for two different values of the Reynolds number: one for $\mathrm{Re} = 500$ and another for $\mathrm{Re} = 2500$. In both cases the Reynolds number is defined as $\mathrm{Re} = \frac{1}{4}L^2\,\Delta\Omega/\nu$. In the first example no steep vorticity gradients are observed, nor any appreciable boundary layer separation. The final stage, at nondimensional time $t = 125$ (one rotation period of the container with respect to the original angular velocity of the container at $t < 0$ corresponds with a dimensionless time $t = 2\pi$) appears to be close to the final viscous decay stage [31]. The second example of spin-up ($\mathrm{Re} = 2500$) shows steep vorticity gradients and the appearance of secondary cells in the four corners of the container ($t = 5$). These cells are gradually destroyed by the strong central core, and the vorticity distribution at $t = 50$ shows that the flow is reaching a more or less viscous decay stage (compare Fig. 6b with Fig. 5a).

Accurate values of the dimensionless vorticity and stream function at several

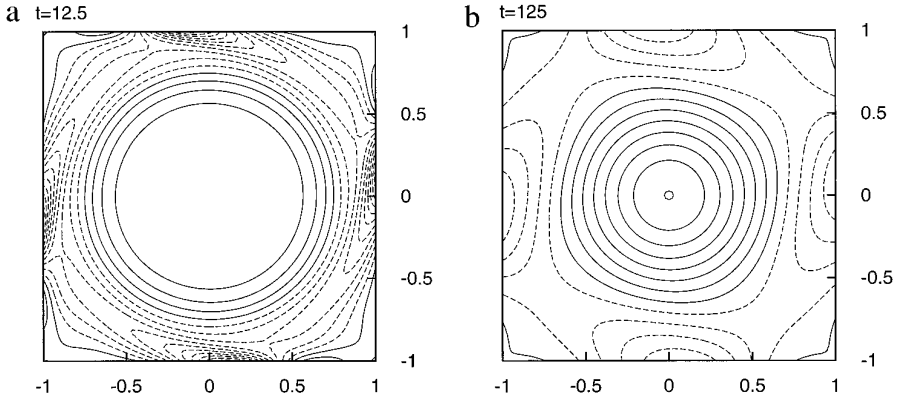

FIG. 5. Some snapshots of the flow evolution during spin-up for Re = 500. Dashed lines represent contours of positive vorticity; drawn lines represent contours of zero or negative vorticity. The vorticity is nondimensionalized by $\Delta\Omega$. The steps between the contours is 0.5 for $t = 12.5$ (a) and 0.025 for $t = 125$ (b). The dimensionless time $t = 2\pi$ corresponds to one rotation period T of the container with respect to the original angular velocity of the container; thus $T = 2\pi/\Delta\Omega$.

times during the spin-up process are listed in Tables II–IV for Re = 500, 1000, and 2500, respectively. The vorticity is made dimensionless by $\Delta\Omega$ and the values of the stream function by $\frac{1}{4}L^2\,\Delta\Omega$.

6.3. *Natural Convection in a Square Cavity*

Finally, another interesting comparison with benchmark computations is possible: simulations of natural convection in a square cavity with adiabatic top and bottom walls based on the 2D Boussinesq equations as performed by De Vahl Davis [32]

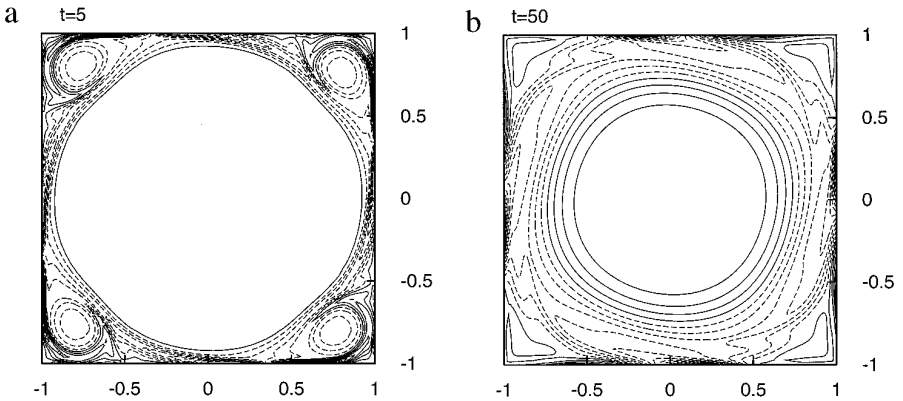

FIG. 6. Some snapshots of the flow evolution during spin-up for Re = 2500. Dashed lines represent contours of positive vorticity; drawn lines represent contours of zero or negative vorticity. The vorticity is nondimensionalized by $\Delta\Omega$. The steps between the contours is 3 for $t = 5$ (a) and 0.5 for $t = 50$ (b). The dimensionless time $t = 2\pi$ corresponds to one rotation period T of the container with respect to the original angular velocity of the container; thus $T = 2\pi/\Delta\Omega$.

TABLE II
Values for the Stream Function and Vorticity at Five Locations in the Container for a Spin-Up Simulation with Re = 500

(x, y)	t	$\psi(x, y)$	$\omega(x, y)$
(0.0, 0.0)	25	-2.566×10^{-1}	-1.913
	50	-1.354×10^{-1}	-1.232
	100	-3.622×10^{-2}	-3.404×10^{-1}
(0.0, 0.4)	25	-1.840×10^{-1}	-1.427
	50	-9.159×10^{-2}	-6.997×10^{-1}
	100	-2.426×10^{-2}	-1.819×10^{-1}
(0.0, 0.8)	25	-3.534×10^{-2}	5.700×10^{-1}
	50	-1.586×10^{-2}	3.188×10^{-1}
	100	-4.014×10^{-3}	1.040×10^{-1}
(0.4, 0.4)	25	-1.227×10^{-1}	-7.551×10^{-1}
	50	-5.864×10^{-2}	-2.706×10^{-1}
	100	-1.560×10^{-2}	-6.551×10^{-2}
(0.8, 0.8)	25	1.085×10^{-3}	3.297×10^{-1}
	50	1.588×10^{-4}	1.460×10^{-1}
	100	-1.099×10^{-4}	3.768×10^{-2}

TABLE III
Values for the Stream Function and Vorticity at Five Locations in the Container for a Spin-Up Simulation with Re = 1000

(x, y)	t	$\psi(x, y)$	$\omega(x, y)$
(0.0, 0.0)	25	-3.410×10^{-1}	-1.999
	50	-2.501×10^{-1}	-1.903
	100	-1.311×10^{-1}	-1.208
(0.0, 0.4)	25	-2.612×10^{-1}	-1.904
	50	-1.781×10^{-1}	-1.397
	100	-8.822×10^{-2}	-6.791×10^{-1}
(0.0, 0.8)	25	-5.834×10^{-2}	6.913×10^{-1}
	50	-3.358×10^{-2}	5.931×10^{-1}
	100	-1.519×10^{-2}	2.989×10^{-1}
(0.4, 0.4)	25	-1.853×10^{-1}	-1.460
	50	-1.176×10^{-1}	-7.145×10^{-1}
	100	-5.597×10^{-2}	-2.539×10^{-1}
(0.8, 0.8)	25	2.358×10^{-3}	4.456×10^{-1}
	50	1.356×10^{-3}	2.805×10^{-1}
	100	4.057×10^{-4}	1.354×10^{-1}

TABLE IV
Values for the Stream Function and Vorticity at Five Locations in the Container for a Spin-Up Simulation with Re = 2500

(x, y)	t	$\psi(x, y)$	$\omega(x, y)$
(0.0, 0.0)	10	-4.538×10^{-1}	-2.000
	20	-4.202×10^{-1}	-2.000
	50	-3.488×10^{-1}	-2.000
(0.0, 0.4)	10	-3.735×10^{-1}	-2.000
	20	-3.391×10^{-1}	-2.000
	50	-2.686×10^{-1}	-1.948
(0.0, 0.8)	10	-1.284×10^{-1}	-1.539
	20	-8.859×10^{-2}	8.124×10^{-1}
	50	-5.785×10^{-2}	9.003×10^{-1}
(0.4, 0.4)	10	-2.949×10^{-1}	-2.000
	20	-2.649×10^{-1}	-1.994
	50	-1.922×10^{-1}	-1.589
(0.8, 0.8)	10	-1.631×10^{-2}	-3.915
	20	-5.445×10^{-3}	-1.956×10^{-1}
	50	1.248×10^{-3}	2.110×10^{-1}

and Le Quéré [33]. This problem is free of any singularity in the boundary conditions, except the presence of the corners. This makes it more attractive than some other problems to test the accuracy of high precision schemes. With the length of this paper in mind only the conclusions of a comparison, based on calculations which are summarized elsewhere [34], are given. The results for the simulations compare within the estimated error of 0.1% with the benchmark simulations by De Vahl Davis, which are obtained with a second-order finite difference scheme and a Richardson extrapolation scheme. The computations compare even exactly with the data presented by Le Quéré, who obtained his results using a pseudospectral Chebyshev algorithm for the Navier–Stokes equations in the primitive variable formulation.

6.4. *Conclusion*

We have shown that it is possible to solve the Navier–Stokes equations in the velocity–vorticity approach by employing spectral methods. The proper relationship between the vorticity and velocity and the requirement that the flow should be divergence-free are enforced with an influence matrix technique, including a tau correction procedure. The influence matrix is nonsingular. The tau correction procedure appeared to be essential in order to avoid catastrophic numerical instabilities. To our knowledge no solution procedure based on a Chebyshev expansion in two nonperiodic directions has been reported in the literature so far for this formulation of the incompressible Navier–Stokes equations.

With the proposed procedure it is possible to obtain machine accurate divergence-free flow fields by either enforcing the vorticity definition or enforcing the continuity equation on the boundary of the computational domain. A minor point of concern from a mathematical point of view is the treatment of the four corner values of the vorticity in the influence matrix when using the approach where the definition of the vorticity is enforced on the boundary. These values are set equal to zero beforehand, which is not entirely justified mathematically. Comparison of the numerical results obtained for 2D-driven cavity flows with data from the literature is satisfactory. There are not many results available with which to compare spin-up simulations, but the present results for low and intermediate Reynolds number show the same features as found with finite difference codes. High Reynolds number simulations of spin-up yield accurate results, despite the singular character of the initial conditions.

An important issue is the extension of influence matrix techniques for application in 3D flow simulations, which is in principle possible. The main problem which has to be solved concerns the considerable increase in size of the influence matrix. Its size is determined by the number of collocation points at the surface of the 3D computational domain. A prohibitively large influence matrix can be avoided by restricting oneself to flows which are periodic in one direction, resulting in 2D influence matrices for each wave number. This approach is employed by, for example, Madabhushi *et al.* [12] for the simulation of the decay of 3D perturbations in a fully laminar flow through a square duct and by Le Quéré and Pécheux who computed convection in a rotating annulus with top and bottom rigid walls [35]. An alternative approach might be the combination of the influence matrix technique and spectral element methods, resulting in one or a few considerably smaller influence matrices. This approach becomes even more advantageous when parallel computing is utilized.

ACKNOWLEDGMENTS

The author wishes to thank GertJan van Heijst for many valuable discussions and for his critical reading of the manuscript and Jeroen van Oijen for performing simulations of natural convection in a square cavity.

REFERENCES

1. H. Fasel, Investigation of the stability of boundary layers by a finite difference model of the Navier–Stokes equations. *J. Fluid Mech.* **78,** 355 (1976).
2. S. C. R. Dennis, D. B. Ingham, and R. N. Cook, Finite difference methods for calculating steady incompressible flows in three dimensions. *J. Comput. Phys.* **33,** 325 (1979).
3. T. B. Gatski, C. E. Grosch, and M. E. Rose, A numerical study of the two-dimensional Navier–Stokes equations in vorticity–velocity variables. *J. Comput. Phys.* **48,** 1 (1982).
4. T. B. Gatski, C. E. Grosch, and M. E. Rose, The numerical solution of the Navier–Stokes equations for 3-dimensional unsteady incompressible flows by compact schemes. *J. Comput. Phys.* **82,** 298 (1989).
5. M. Napolitano and L. A. Catalano, A multigrid solver for the vorticity–velocity Navier–Stokes equations. *Int. J. Numer. Meth. Fluids* **13,** 49 (1991).

6. M. Napolitano and G. Pascazio, A numerical method for the vorticity–velocity Navier–Stokes equations in two and three dimensions. *Comput. Fluids* **19,** 489 (1991).
7. P. Orlandi, Vorticity–velocity formulation for high Re flows. *Comput. Fluids* **15,** 137 (1987).
8. G. Guj and F. Stella, A vorticity–velocity method for the numerical solution of 3D incompressible flows. *J. Comput. Phys.* **106,** 286 (1993).
9. G. Guevremont, W. G. Habashi, P. L. Kotiuga, and M. M. Hafez, Finite element solution of the 3D compressible Navier–Stokes equations by a velocity–vorticity method. *J. Comput. Phys.* **107,** 176 (1993).
10. O. Daube, Resolution of the 2D Navier–Stokes equations in velocity–vorticity form by means of an influence matrix technique. *J. Comput. Phys.* **103,** 402 (1992).
11. L. Quartapelle, *Numerical Solution of the Incompressible Navier–Stokes Equations* (Birkhauser, Basel, 1993).
12. R. K. Madabhushi, S. Balachandar, and S. P. Vanka, A divergence-free Chebyshev collocation procedure for incompressible flows with two non-periodic directions. *J. Comput. Phys.* **105,** 199 (1993).
13. C. G. Speziale, On the advantages of the vorticity–velocity formulation of the equations of fluid dynamics. *J. Comput. Phys.* **73,** 476 (1987).
14. W. Z. Shen and T. P. Loc, Numerical method for unsteady 3D Navier–Stokes equations in velocity–vorticity form. *Comput. Fluids* **26,** 193 (1997).
15. H. D. Nguyen, S. Paik, and J. N. Chung, Application of vorticity integral conditioning to Chebyshev pseudospectral formulation for the Navier–Stokes equations. *J. Comput. Phys.* **106,** 115 (1993).
16. C. Canuto, M. Y. Hussaini, A. Quateroni, and T. A. Zang, *Spectral Methods in Fluid Dynamics* (Springer-Verlag, Berlin, 1987).
17. [Matrix multiplication techniques are more efficient than FFTs when the number of Chebyshev modes is somewhere between 64 and 128]
18. S. A. Orszag, Numerical methods for the simulation of turbulence. *Phys. Fluids, Suppl. II* **12,** 250 (1969).
19. D. B. Haidvogel and T. Zang, The accurate solution of Poisson's equation by expansion in Chebyshev polynomials. *J. Comput. Phys.* **30,** 167 (1979).
20. L. S. Tuckerman, Divergence-free velocity fields in nonperiodic geometries. *J. Comput. Phys.* **80,** 403 (1989).
21. L. Kleiser and U. Schumann, in *Proceedings, Third GAMM Conference on Numerical Methods in Fluid Mechanics,* edited by E. H. Hirschel (Vieweg, Braunschweig, 1980), p. 165.
22. P. S. Marcus, Simulation of Taylor–Couette flow. Part 1. Numerical methods and comparison with experiment. *J. Fluid Mech.* **146,** 45 (1984).
23. P. Le Quéré and T. Alziary de Roquefort, Computation of natural convection in two-dimensional cavities with Chebyshev polynomials. *J. Comput. Phys.* **57,** 210 (1985).
24. P. Le Quéré, R. Masson, and P. Perrot, A Chebyshev collocation algorithm for 2D non-Boussinesq convection. *J. Comp. Phys.* **103,** 320 (1992).
25. J. Werne, Incompressibility and no-slip boundaries in the Chebyshev–tau approximation: Correction to Kleiser and Schumann's influence-matrix solution. *J. Comput. Phys.* **120,** 260 (1995).
26. [The specific choice of the additional source term can be associated with the high frequency residuals in the Navier–Stokes equations in the (**u**, p) formulation]
27. U. Ghia, K. N. Ghia, and C. T. Shin, High-Re solutions for incompressible flow using the Navier–Stokes equations and a multigrid method. *J. Comput. Phys.* **48,** 387 (1982).
28. P. Demaret and M. Deville, Chebyshev collocation solutions of the Navier–Stokes equations using multi-domain decomposition and finite element preconditioning. *J. Comput. Phys.* **95,** 359 (1991).
29. J. Shen, Hopf bifurcation of the unsteady regularized driven cavity flow. *J. Comput. Phys.* **95,** 228 (1991).
30. T. N. Phillips and G. W. Roberts, The treatment of spurious pressure modes in spectral incompressible flow calculations. *J. Comput. Phys.* **105,** 150 (1993).

31. J. A. van de Konijnenberg, Ph.D. thesis, Eindhoven University of Technology, 1995.
32. G. De Vahl Davis, Natural convection of air in a square cavity: a benchmark numerical solution. *Int. J. Numer. Meth. Fluids* **3,** 249 (1983).
33. P. Le Quéré, Accurate solutions to the square thermally driven cavity at high Rayleigh number. *Comp. Fluids* **20,** 29 (1991).
34. J. A. van Oijen, Master's thesis, Eindhoven University of Technology, 1996.
35. P. Le Quéré and J. Pécheux, A three-dimensional pseudo-spectral algorithm for the computation of convection in a rotating annulus, *Spectral and high order methods for partial differential equations,* in *Proceedings, ICOSAHOM '89 Conference, Como, Italy, June 26–29, 1989,* edited by C. Canuto and A. Quarteroni, p. 261.